Erschienen in: Zeitschrift für Physikalische Chemie ; 226 (2012), 7-8. - S. 779-795

Z. Phys. Chem. **226** (2012) 779–795 / **DOI** 10.1524/zpch.2012.0275
© by Oldenbourg Wissenschaftsverlag, München

Probability Densities of a Forced Probe Particle in Glass: Results from Mode Coupling Theory and Simulations of Active Microrheology

By Ch. J. Harrer[1], A. M. Puertas[2], Th. Voigtmann[3], and M. Fuchs[1,*]

[1] Fachbereich Physik, Universität Konstanz, 78457 Konstanz, Germany
[2] Departamento de Física Aplicada, Universidad de Almería, 04.120 Almería, Spain
[3] Zukunftskolleg der Universität Konstanz und Institut für Materialphysik im Weltraum, Deutsches Zentrum für Luft- und Raumfahrt (DLR), Linder Höhe, 51170 Cologne, Germany

Dedicated to Matthias Ballauff on the occasion of his 60th birthday

(Received May 22, 2012; accepted in revised form July 6, 2012)
(Published online August 6, 2012)

Active Micro-Rheology / Glass Transition / Colloidal Suspensions

We investigate the displacements of a probe particle inside a glass, when a strong external force is applied to the probe (active nonlinear microrheology). Calculations within mode coupling theory are presented for glasses of hard spheres and compared to Langevin and Brownian dynamics simulations. Under not too strong forces where the probe remains trapped, the probe density distribution becomes anisotropic. It is shifted towards the direction of the force, develops an enhanced tail in that direction (signalled by a positive skewness), and exhibits different variances along and perpendicular to the force direction. A simple model of an harmonically trapped probe rationalizes the low force limit, with strong strain softening setting in at forces of the order of a few thermal energies per particle radius.

1. Introduction

Many colloidal suspensions are composed of constituents that have typical dimensions in the μm range. One is therefore interested in understanding the dynamical processes occurring in these systems on mesoscopic length scales. A recent experimental technique to obtain such information is called active microrheology [1,2]: one inserts a probe particle, similar in size to the host particles, into the system and subjects it to controlled external driving, such as a (constant) external force. This is conveniently realized in colloids by laser tweezers, magnetic forces, or carefully tailored surface-chemistry reactions [3]. Since scaling arguments imply that thermal fluctuations correspond to forces in the pN range for these colloidal systems, one can easily access the strongly nonlinear-response regime in active microrheology. If analyzed

* Corresponding author. E-mail: matthias.fuchs@uni-konstanz.de

Konstanzer Online-Publikations-System (KOPS)
URL: http://nbn-resolving.de/urn:nbn:de:bsz:352-227136

properly, the nonlinear response of the probe reveals a wealth of information on the dynamics of the host fluid; in particular if the latter shows highly collective relaxation behavior, such as at high densities close to the glass transition [4] or close to jamming [5].

In the fluid, a pulled probe eventually reaches a steady-state velocity, related to the driving force by a friction coefficient ζ. Linear response demands the velocity to be proportional to the force, hence the friction coefficient to be a constant. In active-microrheology experiments on dense colloidal hard-sphere model suspensions [6], a strong nonlinear variation of ζ with the external force $F_{\rm ex}$ was found: strong forces drastically reduce the friction experienced by the probe. The threshold for this "force thinning" effect to set in is at forces much larger than the thermal ones, *i.e.*, $F_{\rm ex} \gg k_{\rm B}T/a$, where a is a typical particle radius and $k_{\rm B}T$ is the thermal energy. This has been related to the cage effect that dominates the relaxation dynamics at high density: the probe particle is trapped by transient cages of nearest neighbors, and the force thinning threshold marks the point where force-induced motion overrules the structural relaxation set by the decaying cages.

The limiting case of this scenario is the response of a pulled probe inside either a jammed state [7] or an ideal glass, *i.e.*, an amorphous solid where the embedding particles no longer relax to thermal equilibrium. The mode-coupling theory of the glass transition (MCT) [8] explains a basic mechanism behind nearest-neighbor cages becoming permanent. The theory has recently been extended to force-driven active microrheology in the nonlinear-response regime [9]. A remarkable consequence was found: in the ideal glass, a force threshold $F_{\rm ex}^{c}$ exists, which marks a transition, from a strictly localized probe in a deformed amorphous solid at low forces, to a local melting leading to delocalization and long-range motion of the probe at large forces. Experiments and computer simulation results in the liquid have successfully been interpreted in the theoretical framework [9,10]. In recent work [11,12], emphasis was placed on understanding the delocalized state, in terms of friction coefficients and fluctuations around the mean trajectory in terms of mean-squared displacements.

In this contribution, we focus instead on the localized region, *i.e.*, on a probe embedded in a frozen random environment, subject to a force that is strong enough to leave the linear response regime, but small enough to keep the probe particle localized. This supplements earlier work studying single particle motion in crystalline environments [13] to the disordered case. We present results of MCT describing the probability densities of probe positions, and discuss some of their basic statistical properties. We compare with results from molecular-dynamics and Brownian-dynamics computer simulations.

2. Methods

2.1 Theory

Let us recall the relevant equations from the microscopic MCT for active nonlinear microrheology [9]. The theory considers the Fourier-transformed probe-particle form factor $f_{\vec{q}}^{s}$ at wave vector $\vec{q}$. It is finite for a probe particle that is trapped in the glass, where it describes the localized probe-density distribution at (infinitely) long times. MCT predicts a transition from a trapped to a delocalized probe upon increasing the

external force, or decreasing the particle interactions. The latter can result from decreasing the host-fluid density, from increasing the temperature of the system, or from making the probe particle smaller. Schematically simplified versions of MCT have been used to analyze such force-induced delocalization transitions in detail [14], and to describe available data such as friction coefficients, density correlation functions, or mean-squared displacements of the probe particle [9,10,12]. These analyses point out that the idealized concept of a forced but still localized probe in a non-relaxing amorphous host solid is very useful in understanding the qualitative nonlinearities observed for probes pulled through dense, complex fluids.

The real-space representation of the form factor $f_{\vec{q}}^s$,

$$f^s(\vec{r}) = \int \frac{\mathrm{d}^3 q}{(2\pi)^3}\, e^{-i\vec{q}\cdot\vec{r}}\; f_{\vec{q}}^s\,, \tag{1}$$

describes the stationary probability for the center of the probe particle to be in an infinitesimal volume element around $\vec{r}$, provided that it was at the origin initially (when the constant external force $\vec{F}_{\mathrm{ex}}$ was switched on). Because of particle conservation, $f^s(\vec{r})$ is normalized to unity. In a quiescent amorphous solid, spatial isotropy is assumed, which is reflected in the fact that $f_{\vec{q}}^s$ depends on the wave vector only through its modulus, $|\vec{q}|$.

Spatial symmetry is broken by the external force: the spherical symmetry is reduced to a rotational one around the force axis (taken to be the z axis in the following), and the distribution in the direction of the force becomes qualitatively different. In particular, it allows for a non-zero mean and, more generally, non-zero odd moments of the distribution – something forbidden by symmetry in the quiescent case. For later reference, recall the standard definitions of the first few moments of $f^s(\vec{r})$: the lowest nontrivial moments are the mean $\langle z\rangle$ along the force direction, the variances $\langle \Delta z^2\rangle$ and $\langle \Delta x^2\rangle$ in direction of and perpendicular to the force, and the skewness of the distribution along the force axis, γ_1:

$$\langle z\rangle = \int \mathrm{d}^3 r\; z\; f^s(\vec{r}) \tag{2a}$$

$$\langle \Delta z^2\rangle = \int \mathrm{d}^3 r\; (z-\langle z\rangle)^2\; f^s(\vec{r}) \tag{2b}$$

$$\langle \Delta x^2\rangle = \int \mathrm{d}^3 r\; x^2\; f^s(\vec{r}) \tag{2c}$$

$$\gamma_1 = \frac{\langle \Delta z^3\rangle}{\langle \Delta z^2\rangle^{3/2}} = \frac{1}{\langle \Delta z^2\rangle^{3/2}} \int \mathrm{d}^3 r\; (z-\langle z\rangle)^3\; f^s(\vec{r}) \tag{2d}$$

MCT decomposes the internal forces acting on the probe into density fluctuations of the probe and its surrounding host liquid, which we take to consist of a colloidal dispersion dissolved in a (featureless) solvent. Because the particle interactions are translational invariant, MCT works with plane-wave decompositions of these fluctuations, and only at the end Fourier back-transforms to real space are taken as in Eq. (1). The form factor $f_{\vec{q}}^s$ appears as the long-time limit of probe-density autocorrelation functions, that do not decay to zero for a localized particle (corresponding to the emergence

of an elastic contribution in the scattering spectrum). Quite generically, one derives

$$f^s_{\vec{q}} = \frac{m^s_{\vec{q}}[f, f^s]}{1 + m^s_{\vec{q}}[f, f^s]} \,. \tag{3}$$

The cage effect appears in the retarded friction and its history-dependence. It is captured in a generalized friction kernel $m^s_{\vec{q}}$ for which exact formal expressions are known that, however, can only be evaluated with approximations. MCT approximates the host-probe force fluctuations using effective interactions provided by the Ornstein–Zernike direct correlation functions. As a consequence, only wavevector-dependent density fluctuations need to be calculated within the theory. The direct correlation functions here are assumed to be known from some separate theory, *e.g.*, density functional or liquid state theory [15]. In the idealized glass, the structure of the host system is then fully encapsulated in f_q, the isotropic collective nonergodicity parameter (Debye-Waller factor, in the case of a monodisperse one-component host). The f_q are real-valued and well known from quiescent MCT calculations [8].

The wavevector-dependent probe form factor $f^s_{\vec{q}}$, the central object of our calculations, then is determined by the MCT closure to Eq. (3), given through the mode-coupling functional [9]

$$m^s_{\vec{q}}[f, f^s] = \int \frac{\mathrm{d}^3k}{8\pi^3} \frac{S^s(p)^2}{nS(p)} \frac{(\vec{q}\cdot\vec{p})\,\omega^s_{\vec{q},\vec{p}}}{\left(\omega^s_{\vec{q},\vec{q}}\right)^2} f_p\, f^s_{\vec{k}} \,. \tag{4}$$

Here, $\vec{p} = \vec{q} - \vec{k}$, and $p = |\vec{p}|$ have been introduced for abbreviation, and the host-liquid particle density is denoted by n. The term $\omega^s_{\vec{q},\vec{p}} = [\vec{q} - i\vec{F}_{\mathrm{ex}}/k_{\mathrm{B}}T]\cdot\vec{p}$ embodies instantaneous forces. $S^s(p)$ and $S(p)$ are the equilibrium static structure factors given by, respectively, the probe-host and the host-liquid interactions, and connected to the mentioned direct correlation functions. The latter structure factor also is the only input into the calculation of the collective nonergodicity parameter f_q within MCT, so that all input to determine $f^s_{\vec{r}}$ is now specified.

While for $F_{\mathrm{ex}} = 0$ the well-studied quiescent MCT follows, finite external forces $\vec{F}_{\mathrm{ex}}$ affect by Newton's laws the momentum balance and thus cause a shift in the wavevector $\vec{q}$ in $\omega_{\vec{q},\vec{p}}$. Because of the displacement of the probe from the origin, its Fourier-transformed distribution $f^s_{\vec{q}}$ is complex. Realness of the real space distribution, however, follows from $f^{s*}_{\vec{q}} = f^s_{-\vec{q}}$, which is a consequence from Eq. (3) to (4), at least for small and intermediate forces. There are indications from numerical solutions of the microscopic MCT equations that at larger forces, a bifurcation takes place to a solution that violates this requirement [16]. In the previous analyses involving schematic models, where no detailed spatial information is kept, this singularity was regularized. Here, we only consider external forces that are smaller than the bifurcation threshold.

Choosing the interactions between particles determines the equilibrium structure information required in Eq. (4), and thus completely specifies the solutions of the MCT equations for active microrheology. We will discuss a system of monodisperse hard spheres with radius a. The dimensionless density is given in terms of the packing fraction, $\varphi = \frac{4\pi}{3}na^3$, which quantifies the volume taken by the spheres relative to the total volume. It is the only control parameter determining the structure of the host system.

For simplicity, we will also consider a probe particle that is identical in size to the surrounding spheres. The Percus-Yevick approximation [15] of the direct correlation functions for hard spheres is used to approximate the MCT coupling coefficients: this liquid-state theory is well established, analytically solvable, and remains reasonable up to high densities. Within this model, MCT predicts a glass transition to occur at a critical packing fraction $\varphi_c \approx 0.516$. We consider the window $\varphi_c \leq \varphi \leq 0.54$ in the following.

Equations (3) and (4) are solved on a discrete lattice of 128×129 points in the magnitude–angle plane, $(|\vec{q}|, \vartheta)$, where ϑ is the angle formed between $\vec{q}$ and $\vec{F}_{ex}$. Angular integration runs over the interval $[0, \pi]$ for the angle ϑ. As $f^s_{\vec{q}}$ is rotationally invariant around the axis of the force it does not depend on the azimuth ϕ. Still integration of this angle over the interval $[0, 2\pi]$ has to be performed when evaluating the mode-coupling functional. Wave-vector modulus integration starts at $2aq_{min} = 0.001$ up to a cutoff $2aq_{max} = 45$, 50, 60, or 65 (for $\varphi = 0.516$, 0.52, 0.53, and 0.54); at larger q, both f_q and $f^s_{\vec{q}}$ have sufficiently decayed to zero. To allow for sufficiently smooth interpolation of f_q, which is pre-determined by equations analogous to Eqs. (3) and (4), the latter was calculated on a grid of 2048 points in $|\vec{q}|$ (angular integration being performed analytically in this case). We found no qualitative dependence on the discretization, checked by some calculations for finer and coarser grids. However, the inverse Fourier transform required by Eq. (1) is very sensitive to cutoff effects, and for the grid used here causes tiny rapid oscillations in $f^s(\vec{r})$ that cause artefacts when calculating moments of the distribution. This is remedied by setting $|f^s(\vec{r})|$ to zero below a threshold of $2.5 \cdot 10^{-4}$.

2.2 Simulations

To conduct first qualitative tests of the predicted features of the density distributions, we also performed computer simulations of active force-driven microrheology. Two model systems were used: strongly damped molecular dynamics for a three-dimensional system of slightly soft spheres based on a Langevin equation, and two-dimensional Brownian dynamics simulations for hard spheres.

The Langevin dynamics simulation has been used extensively before, both in discussing the equilibrium approach to the glass transition [17,18], and for microrheology [9,10]; implementation details are given in these publications. The $3d$ system consists of 1000 purely repulsive particles with a power-law interaction, $V(r) \sim r^{-36}$, and interaction radii that are randomly drawn from a flat distribution of half-width 10% to avoid crystallization. Periodic boundary conditions are used, and the box is elongated by a factor of 8 in the force direction. No finite-size effects were observed by changing the geometry of the box. The glass-transition packing fraction of this system is known to be $\varphi_c \approx 0.595$. Here we show simulations sweeping the external force at a fixed density of $\varphi = 0.57$, accessing the (still transiently) frozen-in component of the probe density distribution at an intermediate time $t \approx 25\sqrt{ma^2/k_BT}$ (m is the particle mass). For this time, the transient self-intermediate scattering functions at $qa \approx 3$ are close to their plateau value [9,10]. Averaging over 300 simulations each consisting of about 40 independent driving cycles was used to improve statistics. Simulations have also been performed at lower densities, and at $\varphi = 0.62$; for the latter, the system can no longer be equilibrated in the available computing time, but has been aged

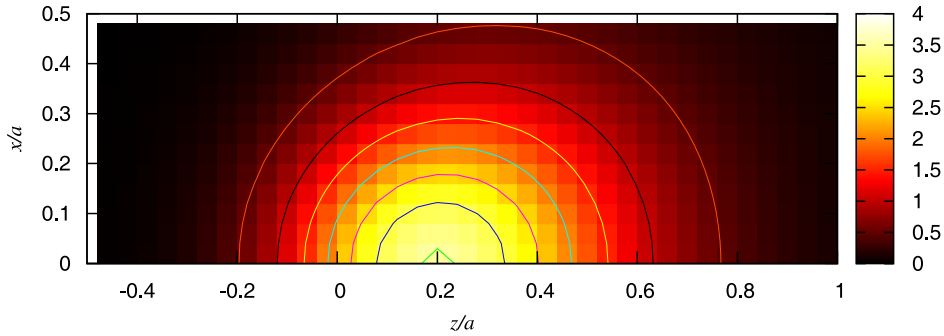

Fig. 1. Contour plot of the probability density of a forced probe-sphere in a hard sphere glass at the glass transition packing fraction, $\varphi_c = 0.516$, as calculated in MCT. The probe-particle and host particles are equal sized (radius a), and the force is $\vec{F}_{ex} = 10\vec{e}_z k_B T/a$. A cut $f^s(x, z, y = 0)$ is shown.

for $t_w = 25\,000\sqrt{ma^2/k_B T}$. Still, with this choice, considerable aging effects cannot be ruled out for $F_{ex} \lesssim 35\, k_B T/a$, making it preferable to obtain the density distributions from the liquid-state simulation as mentioned above.

The Brownian dynamics simulation considers an equimolar binary mixture of hard discs in $d = 2$ dimensions, with radius ratio 1.4. A hybrid Monte-Carlo scheme based on event-driven dynamics [19] is used, where a thermostat is introduced which at every integer-multiple of a 'Brownian time' τ_B redraws all particle velocities from an identical Gaussian distribution. This mimics Brownian motion after many τ_B. Inspired by Carpen and Brady [20], the external force on the probe-particle is implemented by a shift of its Gaussian velocity distribution by the value F_{ex}/ζ_0 in the fixed force direction (ζ_0 is the short time friction coefficient). The glass-transition dynamics of this system has been analyzed in detail [21], establishing $\varphi_c \approx 0.795$. For the reasons explained above, we chose a density $\varphi = 0.78$ and measured the probe-particle distribution function at intermediate times. As a probe particle, a bigger disc is chosen randomly.

3. Results

Figure 1 shows a two-dimensional cut, $f^s(x, z, y = 0)$, of the probability density of the forced probe in a hard sphere glass as calculated within MCT. The packing fraction is the critical one, $\varphi_c = 0.516$, where quiescent MCT locates the formation of an (idealized) glass. Probe and host fluid particles are taken to be identical, which leads to a strong coupling of the probe-particle to the collective fluid density. For vanishing external force, the probe is localized inside nearest-neighbor cages, and due to spatial isotropy its probability density is spherically symmetric and centered around the origin. The width of the distribution is of the order of a tenth of the average particle separation (that is, some fraction of the particle diameter $2a$), as was first discussed by Lindemann in crystals [8,15,22].

For the large force $F_{ex} = 10\, k_B T/a$ shown in Fig. 1, the distribution is shifted to the wall of the cage, and a slight anisotropy between the directions aligned with and opposite to the external force becomes noticeable.

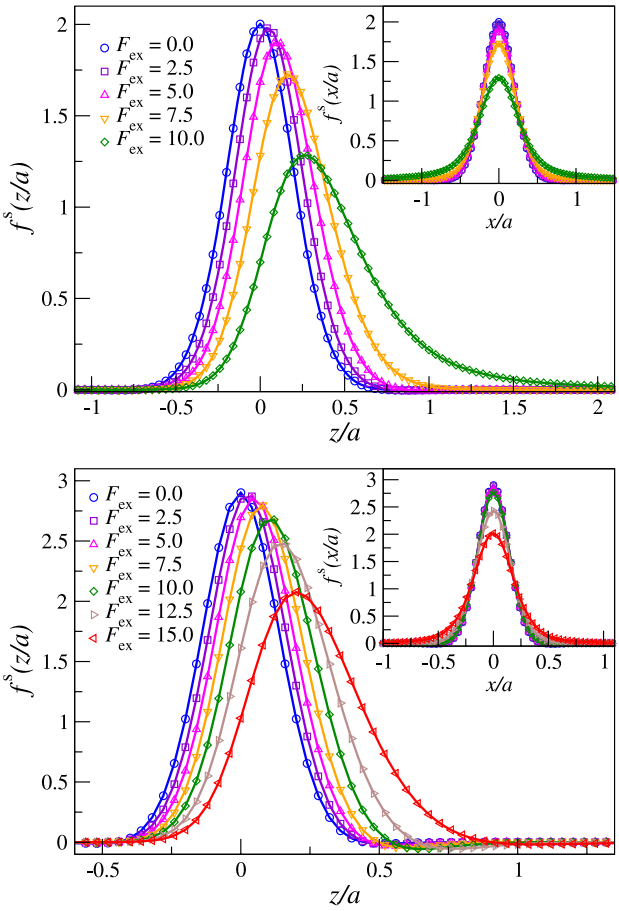

Fig. 2. Stationary density distributions of the probe-particle along the direction of the external force as calculated by MCT, and for forces as labeled in units of $k_B T/a$. Probe and fluid particles have radius a. The upper panel is at the packing fraction of the MCT glass transition, $\varphi_c = 0.516$, the lower one in a glass at $\varphi = 0.53$ (note the different horizontal scales). The insets show the corresponding probability densities along the x-direction perpendicular to the force (with again different horizontal scales).

To identify the anisotropic effects induced by the external force more clearly, it is convenient to discuss the one-dimensional marginal probability densities obtained from integrating out two spatial directions. Of particular interest is $f^s(z)$, the probability distribution along the force axis, shown in Fig. 2 for forces starting from zero up to the value $F_{ex} = 10\, k_B T/a$ shown in Fig. 1, in steps of $2.5\, k_B T/a$. In the insets of Fig. 2, we also show $f^s(x) \equiv f^s(y)$, the marginal distributions along directions perpendicular to the force. We show results for both the glass-transition density, and a state point deeper in the glass, $\varphi = 0.53$, where the probe remains localized for a larger range of forces. The qualitative effects of the external force are the same irrespective of density (as long as one stays inside the glass). Quantitatively, the distributions for the higher density are narrower, reflecting the fact that particles are more tightly localized

in a more densely packed system; note the different horizontal scales in the two panels of Fig. 2.

With increasing force, the half-width at half maximum of the distribution increases, starting from Lindemann's value at zero force. This indicates that cages are continuously widened by applying an increasing external force, in all spatial directions. The center of the distribution along the force axis, $f^s(z)$, shifts in the direction of the force, as is intuitive. Spatial symmetry demands that $f^s(x)$ at the same time remains centered on zero, as verified from the figure.

In $f^s(z)$, a characteristic asymmetry develops, with an increased wing extending in the direction of the force stronger than in the direction opposite to it. Interestingly, also the distributions characterizing the probe probability densities in directions perpendicular to the force show appreciable wings at large forces, extending to distances much larger than Lindemann's length.

Let us remark on one other feature that can be identified for the distributions shown in Fig. 2. For some state points, slightly negative dips can be identified in the MCT calculations. This is clearly unphysical. One has to keep in mind that MCT is formulated in wave-vector space, where it is designed to guarantee a number of exact properties of correlation functions in equilibrium [8]. Since the theory involves approximations, this guarantee however does not carry over to the real-space formulation obtained from Fourier-transforming the MCT results. In fact, small negative contributions in the predicted probability densities (van Hove functions) of a quiescent hard-sphere glass are known [18]; they are thus not a consequence of extending the theory to the nonlinear response. Note that even the equilibrium structure approximation we use as input for our calculations, *viz.* the Percus-Yevick approximation for hard spheres, fails to satisfy exact positivity of the real-space pair distribution functions (albeit at higher densities than we consider) [15]. As Fig. 2 shows, the unphysical negative dips become more pronounced for higher densities, but become weaker and finally (almost) disappear with increasing force. They remain small for all densities $\varphi \leq 0.54$. In the following, we will concentrate on the upper portions of the distribution functions where we expect MCT to make sensible predictions.

From the overall shape of the distributions shown in Fig. 2 it is apparent that their first few moments allow to quantify the mentioned qualitative effects. We now turn to a discussion specifically of the mean, variance, and skewness of $f^s(z)$ and $f^s(x)$. In calculating these quantities, the unphysical negative portions have to be treated with care. In particular, high-order moments tend to emphasize the small errors identified in Fig. 2. We thus introduce an *ad-hoc* correction by setting the negative dips to zero when calculating moments (the distribution is re-normalized afterwards). Values obtained from both the uncorrected and the corrected distributions are shown in the following figures, to allow an assessment of our *ad-hoc* correction.

Figure 3 shows the mean values $\langle z \rangle$ of the probe-displacements in response to the external force $\vec{F}_{\text{ex}}$ for a number of glass states. The curves are continued up to the values of the external force where the mentioned bifurcation in the MCT equations takes place. Beyond this force, which depends on density, we consider the microscopic MCT results not trustworthy. With increasing density, the shift of $\langle z \rangle$ with F_{ex} becomes smaller as the elastic strength of the glass also increases. Initially, $\langle z \rangle$ grows linearly with F_{ex}: this may be called Hookean behavior, and is expected within the general approach of

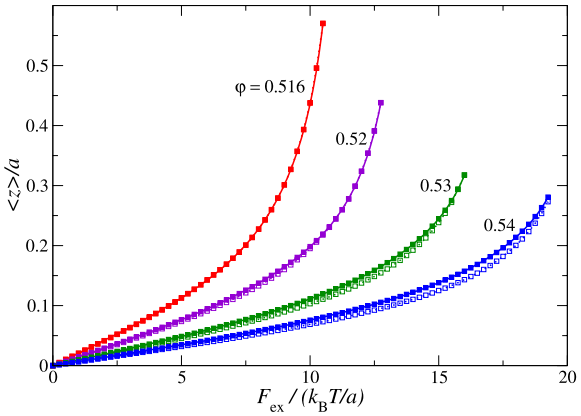

Fig. 3. Mean value $\langle z \rangle$ of the long-time limit of the probe-particle displacement along the force direction as function of the external force F_{ex}. Curves for different glass packing fractions φ are shown as labeled. At the higher two φ, corrected (filled squares) and uncorrected (open squares) $\langle z \rangle$ differ slightly; see text for details.

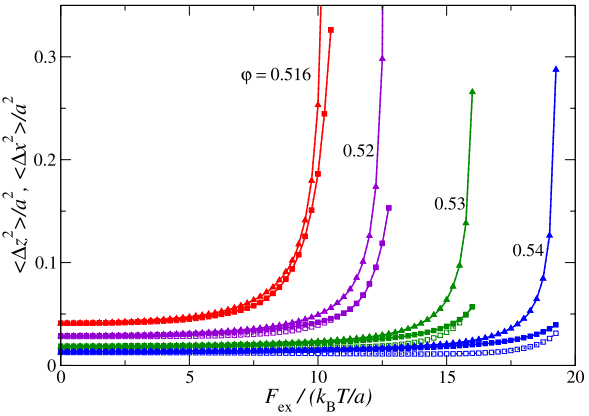

Fig. 4. Variances $\langle \Delta z^2 \rangle$ (squares) and $\langle \Delta x^2 \rangle$ (triangles) of the stationary probe-particle density distribution along, respectively, perpendicular to the force direction as function of the external force F_{ex}. Curves for different glass packing fractions φ are shown as labeled. At the higher two φ the corrected (filled squares) and uncorrected (open squares) $\langle \Delta z^2 \rangle$-data differ slightly; see text for details.

linear-response theory. We discuss this in more detail below, in connection with Fig. 10. Approaching the bifurcation point, a highly nonlinear dependence of $\langle z \rangle$ on F_{ex} is seen. Since $\langle z \rangle$ grows stronger than linearly, one may call this "strain softening". (Reassuringly, the effect of the mentioned *ad-hoc* correction is small and only becomes visible for the highest densities considered here.)

Figure 4 shows the variances defined in Eq. (2) as functions of the strength of the external force for the four glass densities used above. Again, corrected and uncorrected values agree quite well except for small differences in $\langle \Delta z^2 \rangle$ at the highest densities. At

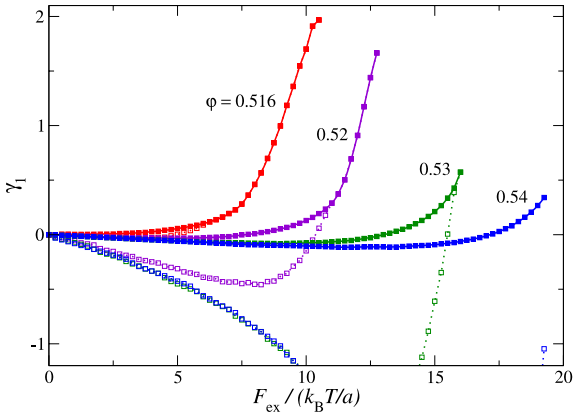

Fig. 5. Skewness γ_1 of the probe-particle density distribution along the force direction as function of the external force F_{ex}. Curves for different glass packing fractions φ are shown as labeled. At all φ except for the lowest one, corrected (filled squares) and uncorrected (open squares) γ_1 differ, because the latter are affected by the (small) negative tails in $f^s(z)$ predicted by MCT. Thus, we judge the corrected ones more reliable; see text for details.

small F_{ex}, the probe-particle response remains nearly isotropic, as required by linear response. Both $\langle \Delta z^2 \rangle$ and $\langle \Delta x^2 \rangle$ approach for $F_{ex} \to 0$ values given by the localization length of the quiescent glass, r_s. This quantity has been evaluated before [8] and has been connected to the Lindemann criterion already mentioned: the localization length r_s of single particles inside a crystal cannot exceed some fraction of the lattice constant, as long as the crystal is supposed to be stable against thermal fluctuations [22]. MCT transfers this concept to a disordered solid, where the average particle separation plays the role of the relevant length scale. The value $\langle \Delta z^2 \rangle = 2r_s^2 \approx 0.04a^2$ at the transition density φ_c has already been verified by dynamic light scattering experiments on hard-sphere-model colloidal suspensions [23,24] and by simulations [17]. In these cases, the time-dependent mean-squared displacement $\langle \delta r^2(t) \rangle$ was studied, whose long-time limit in the glass is $\langle \delta r^2(t = \infty) \rangle = 3\langle \Delta z^2 \rangle$ assuming spatial isotropy.

For increasing force F_{ex}, Fig. 4 confirms the qualitative judgement of Fig. 2: the probe-particle distributions become wider in all directions, revealing a rather steep increase as the bifurcation force is approached from below. Outside the linear-response regime, the response also becomes anisotropic. The distribution perpendicular to the force direction becomes wider more quickly than along the force. We attribute this effect to the wide tails seen in the insets of Fig. 2.

We next discuss the skewness of the distributions, Fig. 5. Here, the small negative dips in the MCT approximation to the real-space distribution functions are amplified so that the uncorrected values of γ_1 become strongly negative for large densities and strong forces. The *ad-hoc* corrected values remain small at small forces and then are positive and increase appreciably for larger F_{ex}; since we expect MCT to work best for the central features of the distribution we consider these latter values to be more accurate. Generically, the marginal distribution $f^s(z)$ is hence right-skewed, *i.e.*, its mass is concentrated to values lower than the mean, indicating that a few realizations corres-

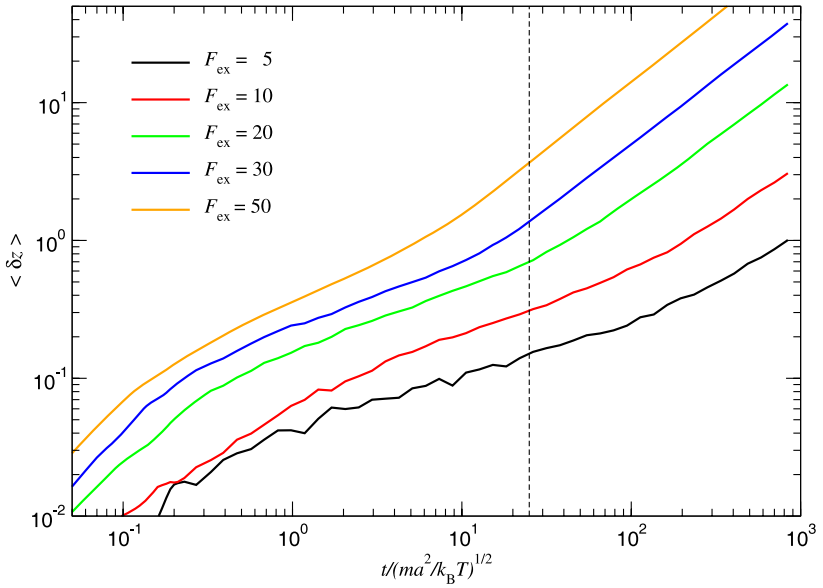

Fig. 6. Linear displacement of the forced tracer particle in direction of the force (given in k_BT/a) for the density $\varphi = 0.57$ from Langevin dynamics simulations. The intermediate time $t = 25\sqrt{ma^2/k_BT}$ at which probe-particle distributions were sampled is indicated by the dashed vertical line.

pond to large excursions in the direction of the force. This is most prominent close to the bifurcation point, where again the most steep increase is seen.

4. Discussion

4.1 Preliminary comparison with simulations

In order to compare with computer simulation, we face the problem that the idealized glass state considered by MCT cannot be obtained in the simulation: at high densities, the system can no longer be equilibrated in the available computer time, and aging effects prevail that are outside the scope of our discussion. We hence choose a density close to the MCT glass transition, where the random host structure still relaxes in the simulation time window. Before this final relaxation sets in, the intermediate nearly-frozen structure can be probed.

To demonstrate this, Fig. 6 shows the linear displacement $\langle \delta z \rangle(t)$ of the probe particle as a function of time since switching on the external force, obtained from the Langevin-dynamics simulation. One recognizes that these functions grow linearly with time at large t, indicating fluid-like steady-state motion corresponding to a finite friction coefficient ζ. This steady state is reached on a time scale governed by the host-fluid relaxation at small forces. Before that, $\langle \delta z \rangle(t)$ exhibits a shoulder as a function of $\log t$, indicative of transient localization. We pick an intermediate time $t = 25\sqrt{ma^2/k_BT}$ (indicated by a dashed line in Fig. 6) where probe-particle distributions are sampled. At this time, the probe particle has fully explored its cage, but is still sufficiently close to its

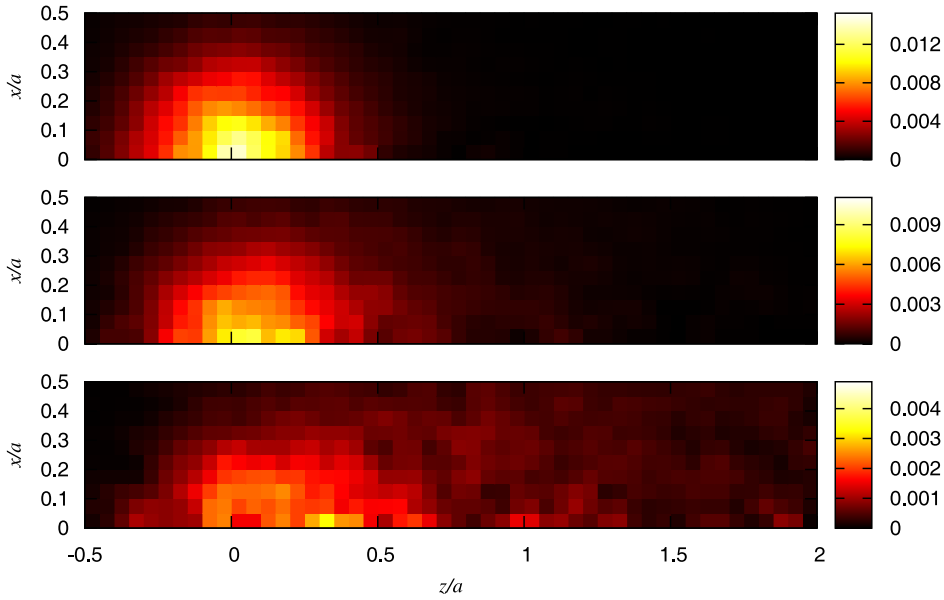

Fig. 7. Probability density of a forced probe in a polydisperse hard sphere fluid at $\varphi = 0.57$ from Langevin dynamics simulations. From top to bottom: $F_{ex}/(k_B T/a) = 10$, 20, and 30; here the force is along the x-axis. The colour code for the unnormalized distribution is given to the right of the respective panel. The time since switching-on the force is chosen such that the localized density distribution is close to its frozen-in form at the glass transition.

transient localized state for a range of low forces, roughly $F_{ex} \leq 20 k_B T/a$. For the higher forces, the time when the probe is pulled out-off the cage moves to shorter values, and the probability distribution sampled at $t = 25\sqrt{ma^2/k_B T}$ becomes characteristic for the delocalized state. For $F_{ex} > 20 k_B T/a$ at the given packing fraction ($\varphi = 0.57$) the simulation results for f^s thus will contain different phenomena than discussed from the theory.

Figure 7 shows the probe-particle distribution $f^s(\vec{r})$ sampled at that time, for various external forces. As in Fig. 2, a cut in a plane containing F_{ex} has been chosen, and rotational symmetry around that axis has been used to improve statistics. The panels correspond to increasing external force. One notices the nearly intact spherical symmetry for the lowest force, $F_{ex} = 10\, k_B T/a$, which is broken for the larger forces. Qualitatively, one recognizes the features discussed above from the MCT predictions: an increasing shift of the center of the distribution in the direction of the applied force, and an increase in the variance in all spatial directions.

The heterogeneity of the probe dynamics is parametrized by the skewness of these distributions in Fig. 8, as defined in Eq. (2d). Increasing the external force from zero, the skewness increases, before it reaches a maximum at intermediate forces and finally decays to zero again. From the above discussion of Fig. 6 and a comparison with the mean probe velocity [9], we associate this decay with the eventual delocalization of the probe; this effect is not contained for the small forces discussed within MCT above. There is qualitative agreement between theory and simulation for the initial increase:

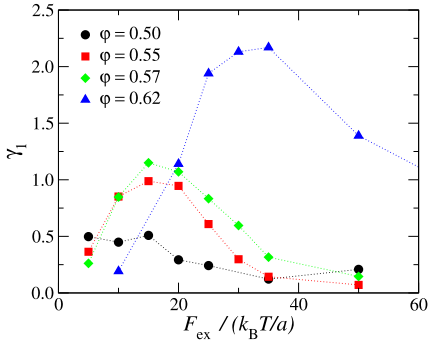

Fig. 8. Langevin simulation results for the skewness γ_1 of the probability distribution along the force-direction as a function of the force, for different densities as labeled.

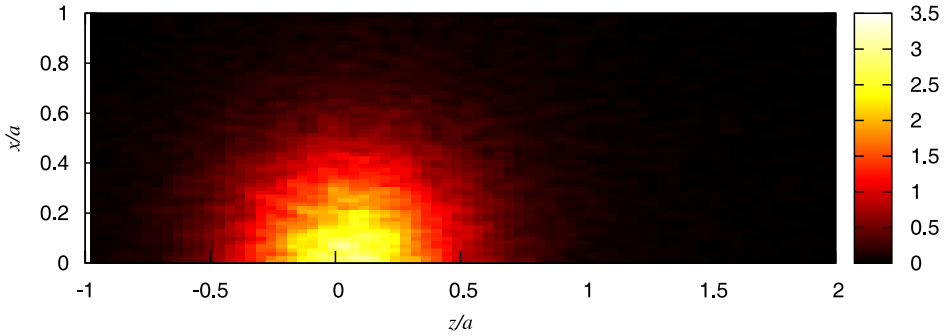

Fig. 9. Probability density of a forced probe in a binary hard disk mixture (radius ratio $a_b/a_s = 1.4$) in $d = 2$ dimensions close to the glass transition density from Brownian dynamics simulations. The probe has been chosen among the bigger disks, the applied force is $F_{ex} = 42 k_B T/a$ in z-direction and $a = 0.6$ denotes the average particle radius. The colour code gives the probability. The time since switching-on the force is chosen such, that the localized density distribution is close to its frozen-in form at the glass transition.

The skewness is positive, indicating that the probe undergoes rare excursions far in the direction of the force, *i.e.*, the density distribution develops a tail there. While in the fluid, the maximum of γ_1 lies at the same force, in the glass the increase shifts to larger forces. This is compatible with the MCT scenario of a critical bifurcation force whose value in the fluid close to the glass transition is given by the one at the transition. Values of $\gamma_1 \approx 1$ at forces around $F_{ex} \approx 10\, k_B T/a$ at the glass transition density are found in MCT; this is in semi-quantitative agreement with the simulations.

Also the two-dimensional Brownian dynamics simulations of active microrheology, broadly give results in agreement with the theoretical predictions. Figure 9 shows a contour plot of the density distribution of a probe (one of the larger species) trapped in an equimolar mixture of disks with radii-ratio $a_b/a_s = 1.4$. The density is close to the glass transition one, and a large force $F_{ex} = 42 k_B T/a$ is applied. Here a denotes the average particle radius $a = (a_b + a_s)/2$. Estimates of the low-order moments, $\langle z \rangle \approx 0.14a$, $\langle \Delta z^2 \rangle \approx 0.32a^2$, $\langle \Delta x^2 \rangle \approx 0.24a^2$, and $\gamma_1 \approx 2.51$ lead to values which can be taken as

extrapolations of the theoretical trends to such strong forces; the small average displacement is noteworthy though, and presumably due to the lower spatial dimension. The asymmetry of the density distribution along the force direction is apparent already from the contour plot.

4.2 Small force model of an harmonically trapped probe

To place the findings reported above in theoretical context, we briefly discuss the linear-response theory of a forced particle in a glass. A prototypical model system is that of a Brownian particle in a harmonic trap. Considering for simplicity only the force direction, there holds the Langevin equation

$$\zeta \dot{u}(t) = -k\,(u(t) - u_0) + F_{\rm ex} + f(t)\,. \tag{5}$$

Here, $u(t)$ is the displacement variable of the particle, and k the spring constant of the harmonic potential. Random forces f are assumed to be Gaussian white noise obeying the fluctuation-dissipation theorem connected to the friction coefficient ζ. The minimum position of the potential is given by u_0. The distance from this minimum, $\delta u = u(t) - u_0$ immediately gives the linear shift and the equal-time variance of the displacement at infinite times,

$$\langle \delta u \rangle^{\rm gl} = \frac{F_{\rm ex}}{k}\,, \qquad \langle \delta u^2 \rangle^{\rm gl}\big|_{F_{\rm ex}=0} = \frac{k_{\rm B}T}{k}\,. \tag{6}$$

Yet, the glass state is not an equilibrium state, but a metastable state, where ergodicity has been broken. The nonergodicity parameters f_q of MCT quantify this, and a finite localization length $r_s = \sqrt{\langle \delta z^2(t \to \infty)\rangle/2}$ is the simplest example of a nonergodic quantity in the probe dynamics. Importantly, the localization length is measured in the limit of infinite times, where the maximal excursion $\delta z(t) = z(t) - z(0)$ of the tracer can be obtained. The question arises how to define ergodic, close to (metastable) equilibrium fluctuation functions in the glass state, which are assumed in the simple harmonic oscillator model. Recently, in the context of measuring strain fluctuations in colloidal glass by microscopy, this problem has been solved [25]. The stationary (quasi-equilibrium) displacement auto-correlation function in the glass state is defined from the mean squared displacement defined in the fluid state by

$$\langle \delta u(t)\delta u(0)\rangle^{\rm gl} = \frac{1}{2}\left(\langle \Delta z^2\rangle - \langle (z(t) - z(0))^2\rangle\right)\,. \tag{7}$$

Here averages on the right are performed using the Gibbs-Boltzmann distribution of the fluid state, while the average on the left hand side is within the compartment in phase space corresponding to the nonergodic glass state. The function $\langle \delta u(t)\delta u(0)\rangle^{\rm gl}$ defined on the left hand side obeys all the properties required of an auto-correlation function, at least if the approximate MCT equations of motion are taken as basis [25]. Clearly and as expected, Eq. (7) gives a linear relation between the displacement $u(t)$ of the probe in the glass and the position $z(t)$, whose long time distribution functions were the topic of our MCT calculations: $u(t) = z(t)$. Somewhat more surprisingly, the second moment

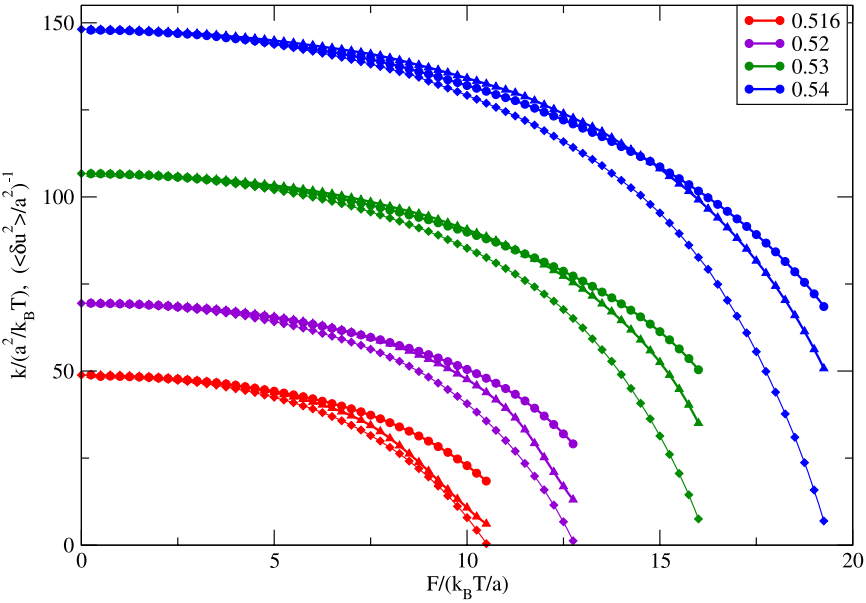

Fig. 10. Effective force constant k (circles) determined from the probe-particle displacement under force for different glass packing fractions φ as listed in the legend. Testing the linear response relation Eq. (6), the displacement variances along $k_BT/\langle\delta u_z^2\rangle^{gl} = 2k_BT/\langle\Delta z^2\rangle$ (triangles) and $k_BT/\langle\delta u_x^2\rangle^{gl} = 2k_BT/\langle\Delta x^2\rangle$ (squares) perpendicular to the force are compared to $k = F_{ex}/\langle\delta u\rangle = F_{ex}/\langle z\rangle$. For small forces, where $\langle\delta u^2\rangle^{gl} \to r_s^2$ isotropically, linear response and the equipartition theorem hold. Shown are only the corrected values not affected by the (small) negative tails in $f^s(z)$ predicted by MCT; see text for details.

of the displacement taken at equal time follows to be half as big as the variance of the density distribution remaining at long times:

$$\langle\delta u^2\rangle^{gl} = \langle(\delta u(t=0))^2\rangle^{gl} = \frac{1}{2}\,\langle\Delta z^2\rangle = \frac{1}{2}\,\langle(z(t\to\infty) - z(0))^2\rangle\,. \tag{8}$$

Figure 10 tests the thus obtained simple model of the motion of the trapped probe in glass. The values of the effective spring constant, $k = F_{ex}/\langle z\rangle$, are compared to the appropriately inverted mean squared displacements $\langle\delta u^2\rangle^{gl}$, namely $k_BT/\langle\delta u^2\rangle^{gl}$, and quantitative agreement is found. This supports the above definition of a displacement fluctuation function in the nonergodic glass state. Its behavior at small forces reduces to the simple model of an equilibrium harmonic oscillator. At larger external forces, force thinning sets in, and the first and second displacement moments behave qualitatively similar, yet quantitatively differ. (In order to eliminate spurious non-monotonic behavior arising from the negative probabilities MCT would predict, only the corrected moments, where the negative probabilities were set to zero, are shown in Fig. 10.)

The linear-response spring constant evaluated by MCT close to the glass transition is $k \approx 50\,k_BT/a^2$, which agrees quite well with a recent estimate $k \approx 80\,k_BT/a^2$ obtained employing a parabolic trap in the Langevin simulations [26]. Following basic elasticity theory, it can be related to a (local) Young's modulus E of the glass. Another rele-

vant length enters this conversion (the cross-section over which the force is applied divided by the original length of the strained object). Assuming this to be roughly a again, we get $E_{\mathrm{micro}} \approx 50\, k_{\mathrm{B}}T/a^3$. In the linear macroscopic rheology of glasses, MCT predicts both the longitudinal and the shear modulus, M and G; for a hard-sphere system at the glass transition, $G \approx 20\, k_{\mathrm{B}}T/(2a)^3$ and $M = M_0 + \delta M \approx 130\, k_{\mathrm{B}}T/(2a)^3$, where $\delta M \approx 55\, k_{\mathrm{B}}T/(2a)^3$ is the nonergodic contribution [27]. From the standard relation between the elastic moduli, $E = (G/M)(1-(4/3)(G/M))/(1-(G/M))$, one gets $E \approx 56\, k_{\mathrm{B}}T/a^3$, which compares reasonably well with the microscopic spring constant.

5. Conclusions

We investigated the nonlinear response of a single particle subject to a strong external force in an amorphous solid. Calculations based on the mode-coupling theory for active nonlinear microrheology allow to access the density distribution functions describing the average probe position in the nonequilibrium system. These distribution functions become asymmetric and loose the spherical symmetry present in the spatially homogeneous equilibrium state: quite intuitively, the center of the distribution is shifted in the direction of the applied force. In addition, two nontrivial effects are predicted: the distribution is widened in all spatial directions, *i.e.*, its localization also perpendicular to the applied force becomes less strong when the force is increased. Further, one identifies strong tails in the distribution function, and in particular a pronounced tail extending along the force from the initial positions, as manifested in a positive skewness parameter. This tail becomes stronger as the force approaches a critical bifurcation threshold. It quantifies dynamical heterogeneities that arise because occasionally particle trajectories follow realizations with large excursions. In fact, it is seen in the simulation that the probe-particle dynamics close to delocalization becomes intermittent. The connection of the strong tails and the bifurcation force found in the MCT equations is currently under investigation.

For small forces, linear response theory allows to understand the results if one takes into account the broken ergodicity of the glass. This proper definition of quasi-equilibrium displacement correlation functions in glass accounts for an otherwise puzzling factor 2 connecting the variance of the probe-distribution functions to the harmonic spring constant characterizing the local rigidity of the nearest-neighbor cage. Semi-quantitatively, the local measure of rigidity can be connected to the macroscopic elastic constants of the glass.

Acknowledgement

We thank for funding by the Deutsche Forschungsgemeinschaft throuh SFB Transregio TR6 and Research Unit FOR 1394. Th. V. thanks for funding through the Helmholtz-Forschungsgemeinschaft (Impuls- und Vernetzungsfonds, VH-NG-406), and through the Zukunftskolleg der Universität Konstanz. A. M. P. acknowledges financial support from Junta de Andalucia and FEDER, and Ministerio de Ciencia e Innovación under projects P09- FQM-4938 and MAT2011-28385, respectively.

References

1. T. A. Waigh, Rep. Prog. Phys. **68** (2005) 685.
2. T. M. Squires and T. G. Mason, Annu. Rev. Fluid Mech. **42** (2010) 413.
3. A. Erbe, M. Zientara, L. Baraban, C. Kreidler, and P. Leiderer, J. Phys.: Condens. Matter **20** (2008) 404215.
4. M. Siebenbürger, M. Fuchs, and M. Ballauff, Soft Matter **8** (2012) 4014.
5. R. Candelier and O. Dauchot, Phys. Rev. E **81** (2010) 011304.
6. P. Habdas, D. Schaar, A. C. Levitt, and E. R. Weeks, Europhys. Lett. **67** (2004) 477.
7. C. J. O. Reichhardt and C. Reichhardt, Phys. Rev. E **82** (2010) 051306.
8. W. Götze, *Complex Dynamics of Glass-Forming Liquids*, Oxford University Press, New York (2009).
9. I. Gazuz, A. M. Puertas, Th. Voigtmann, and M. Fuchs, Phys. Rev. Lett. **102** (2009) 248302.
10. M. V. Gnann, I. Gazuz, A. M. Puertas, M. Fuchs, and Th. Voigtmann, Soft Matter **7** (2011) 1390.
11. D. Winter, J. Horbach, P. Virnau, and K. Binder, Phys. Rev. Lett. **108** (2012) 028303.
12. Ch. J. Harrer, D. Winter, J. Horbach, M. Fuchs, and Th. Voigtmann, J. Phys.: Condens. Matter **24** (2012) 428429.
13. Y. N. Ohshima and I. Nishio, J. Chem. Phys. **114** (2001) 8649.
14. M. V. Gnann and Th. Voigtmann, Phys. Rev. E, in print (2012).
15. J. P. Hansen and I. R. McDonald, *Theory of Simple Liquids*, Academic Press, London (1986).
16. Ch. J. Harrer, in preparation, 2013.
17. Th. Voigtmann, A. M. Puertas, and M. Fuchs, Phys. Rev. E **70** (2004) 061506.
18. F. Weysser, A. M. Puertas, M. Fuchs, and Th. Voigtmann, Phys. Rev. E **82** (2010) 011504.
19. A. Scala, Th. Voigtmann, and C. D. Michele, J. Chem. Phys. **126** (2007) 134109, ISSN 00219606.
20. I. C. Carpen and J. F. Brady, J. Rheol. **49** (2005) 1483.
21. F. Weysser and D. Hajnal, Phys. Rev. E **83** (2011) 041503.
22. F. A. Lindemann, Phys. Z. **11** (1910) 609.
23. W. van Megen, T. C. Mortensen, S. R. Williams, and J. Müller, Phys. Rev. E **58** (1998) 6073.
24. M. Sperl, Phys. Rev. E **71** (2005) 060401.
25. C. L. Klix, F. Ebert, F. Weysser, M. Fuchs, G. Maret, and P. Keim, Phys. Rev. submitted, ArXiv:1108.2636 (preprint 1108.2636) (2011).
26. A. M. Puertas, AIP. Conf. Proc. **1319** (2010) 141.
27. W. Götze and Th. Voigtmann, Phys. Rev. E **67** (2003) 021502.